

Magnification of photonic crystal fluorescence enhancement via TM resonance excitation and TE resonance extraction on a dielectric nanorod surface

This article has been downloaded from IOPscience. Please scroll down to see the full text article.

2010 Nanotechnology 21 125203

(<http://iopscience.iop.org/0957-4484/21/12/125203>)

View [the table of contents for this issue](#), or go to the [journal homepage](#) for more

Download details:

IP Address: 128.174.190.216

The article was downloaded on 22/04/2010 at 22:02

Please note that [terms and conditions apply](#).

Magnification of photonic crystal fluorescence enhancement via TM resonance excitation and TE resonance extraction on a dielectric nanorod surface

Hsin-Yu Wu¹, Wei Zhang², Patrick C Mathias³ and Brian T Cunningham^{1,3,4}

¹ Department of Electrical and Computer Engineering, University of Illinois at Urbana-Champaign, 1406 W Green Street, Urbana, IL 61801, USA

² Department of Material Science and Engineering, University of Illinois at Urbana-Champaign, 1304 W Green Street, Urbana, IL 61801, USA

³ Department of Bioengineering, University of Illinois at Urbana-Champaign, 1304 W Springfield Avenue, Urbana, IL 61801, USA

E-mail: bcunning@illinois.edu

Received 21 October 2009, in final form 9 February 2010

Published 2 March 2010

Online at stacks.iop.org/Nano/21/125203

Abstract

Using a one-dimensional grating surface photonic crystal (PC), we experimentally demonstrate that the detection of fluorescent molecules on a PC surface can be substantially magnified through the combined effects of resonance-enhanced excitation of the fluorescent dye, resonance-enhanced extraction of the fluorescence emission and a dielectric nanorod surface coating increasing the surface area available for fluorophore–PC interaction. Enhanced excitation is obtained by engineering a high- Q TM resonant mode to efficiently couple with an incident TM-polarized $\lambda = 633$ nm laser for exciting Cyanine-5 (Cy5). Enhanced extraction results from a low- Q TE resonance designed to spectrally overlap the Cy5 emission spectrum for channeling TE-polarized emission towards the detection instrument. The entire PC surface is coated with a porous film of TiO₂ nanorods that allows more fluorophores to penetrate into the region of enhanced near-electric fields. Experimental results reveal a 588-fold enhancement in fluorescence intensity relative to an unpatterned glass surface.

(Some figures in this article are in colour only in the electronic version)

1. Introduction

Fluorescence-based biological assays are used widely for measurements in life-science research, clinical diagnostic tests and drug discovery, with applications that include DNA gene expression analysis, protein microarrays for disease biomarker detection and cell imaging. For many of these applications, there is interest in driving the limits of detection to the lowest possible concentration and increasing the signal-to-noise ratio of fluorescence intensity above the background noise. Therefore, an intense area of research is the development of techniques with the ability to enhance fluorescence yield

through increasing the electric-field intensity experienced by fluorescent dyes [1], increasing the collection efficiency of fluorescence emission [2], decreasing the fluorescent lifetime of excited dye molecules [3] and increasing the interaction volume of electric field–fluorophore interaction [4]. Such techniques include metal nanoparticle surfaces [5], metal nanorods [6], metal-coated nanoshells [7] and dielectric-based photonic crystals (PC) [8]. PC-based fluorescence enhancement offers advantages that include the ability to engineer a surface structure with resonances at multiple wavelengths [9] from low-loss, non-quenching, dielectric materials that enable high- Q resonances that support high surface electric-field intensity.

⁴ Author to whom any correspondence should be addressed.

Fluorescence enhancement can be applied to quantitative bioassays by applying surface-bound probe molecules such as DNA or antibodies to the PC and specifically capturing fluorescently labeled biomolecules. With this method, the fluorescent signal from molecules bound to the PC surface is proportional to its concentration in the sample. Previous reports of PC-enhanced fluorescence (PCEF) surfaces have included demonstrations of DNA microarrays [10] and protein immunoassays [11] using organic dyes, and enhanced detection of quantum dots [12]. PCEF utilizes structures designed to produce guided-mode resonance (GMR). The GMR effect occurs when higher (evanescent) diffracted orders of a periodic sub-wavelength surface structure couple to the modes with the highest effective refractive index (RI) [13]. The energy coupled to ‘leaky guided modes’ radiates out from the structure due to its diffractive nature, for forward (transmitted) and backward (specular) diffracted waves with a complex propagation vector perpendicular to the periodic structure. These leaky waves interfere destructively with the directly transmitted zeroth-order diffracted wave and constructively with the specularly reflected zeroth-order diffracted wave, leading to a strong reflection about a resonant wavelength whose linewidth and spectral location are set by the physical parameters of the device. Like other optical resonances, the GMR effect leads to storage of energy within the resonator under steady-state operational conditions, the magnitude of which is directly related to the resonance quality factor, which in turn is inversely related to the resonance linewidth. A high resonance Q factor leads to high intensity near-fields with which fluorophores can interact and fluoresce with greater intensity.

We previously demonstrated that a fluorescence enhancement of $114\times$ can be achieved by incorporating a porous nanorod (NR) structure deposited by the glancing angle deposition (GLAD) technique on a dense nonporous high RI TiO_2 layer of a PC [4]. We also demonstrated an enhancement of up to $193\times$ by allowing fluorophores to penetrate into an exclusively NR-structured high RI TiO_2 layer on a PC surface [14]. The enhancement factor achieved in these previous reports was limited, because a low- Q TE resonance ($Q \sim 33$ in air, $Q \sim 150$ in water) was used to excite fluorophores. In this paper, we demonstrate that a 588-fold enhancement in fluorescence intensity can be achieved relative to an unpatterned glass slide by using three mechanisms together: (1) a narrowband TM resonance with a Q factor of 308 spectrally overlapping the Cy5 absorption spectrum intentionally designed to coincide with the incident TM-polarized laser wavelength for efficiently exciting Cy5, (2) a broadband TE resonance with a Q factor of 39 spectrally overlapping the Cy5 emission spectrum for efficiently redirecting TE-polarized fluorescence emitted by Cy5 toward the detection instrument and (3) a porous GLAD-deposited layer of dielectric TiO_2 NRs on the PC surface to provide greater surface area for adsorption of fluorescent analytes within the volume where the resonant electric-field coupling between the PC and the fluorophore is greatest.

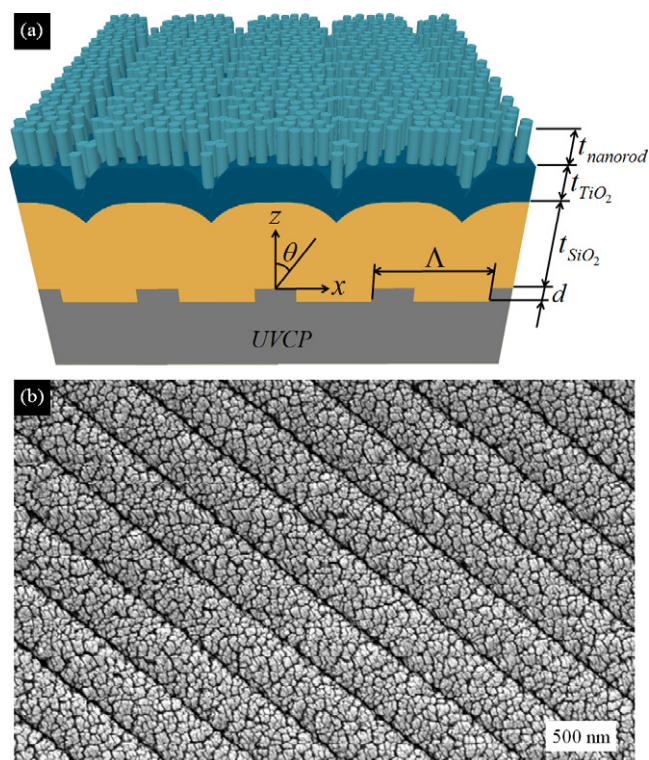


Figure 1. (a) Schematic cross section of the PC. The dimensions are as follows: period $\Lambda = 360$ nm, grating depth $d = 60$ nm, SiO_2 thickness $t_{\text{SiO}_2} = 300$ nm, TiO_2 thickness $t_{\text{TiO}_2} = 160$ nm and NR-structured TiO_2 thickness $t_{\text{nanorod}} = 80$ nm. The grating duty cycle is 50% and the incident angle is labeled as θ . (b) SEM image of top view of an NR-coated PC with 80 nm of NR TiO_2 .

2. Experimental details

2.1. Device fabrication

Figure 1(a) shows a schematic cross section of the PC. We used a nanoreplica molding process to fabricate a linear grating structure with a period of 360 nm (50% duty cycle) and a depth of 60 nm in a low RI UV-cured polymer (UVCP) ($n_{\text{UVCP}} = 1.46$). Next, a 300 nm SiO_2 layer ($n_{\text{SiO}_2} = 1.46$) was deposited by sputter deposition to serve as a spacer layer to prevent the evanescent electric field from extending into the UVCP layer in order to reduce undesirable background fluorescence from the UVCP material. A high RI TiO_2 dense thin film with a thickness of 140 nm ($n_{\text{TiO}_2} = 2.3$) was next deposited by sputter deposition, followed by the NR-structured TiO_2 film, deposited by the GLAD technique in an electron-beam deposition system (Temescal) [15, 16]. The GLAD-deposited TiO_2 had a depth of 80 nm, with an NR diameter of 30 nm, resulting in an effective RI of $n_{\text{nanorod}} = 1.46$ measured by spectroscopic ellipsometry (Woolam). To ensure equivalence of the surface chemistry layers for the PC surface and glass slides used as an experimental reference, a 20 nm dense thin film of TiO_2 was deposited onto the unpatterned glass microscope slides used in this study. Moreover, in order to calculate both enhanced extraction and the surface area effect on the enhancement factor, the same NR-structured TiO_2 film as PCs was deposited onto one of these TiO_2 -coated glass slides as an additional reference. Figure 1(b) shows a

scanning electron microscopy (SEM) image of the top view of the fabricated PC showing NRs uniformly coated onto the grating structure of a PC.

2.2. Surface chemistry process and assay protocol

In preparation for attachment of fluorescent-tagged protein, PCs, NR-coated glass slides and unpatterned reference glass slides were initially cleaned in O₂ plasma for 3 min. An amine-rich surface was provided by immersion in a 1% mixture of amine polymer solution (SRU Biosystems), incubated at room temperature for 24 h, and then washed with ultrapure water. Afterward, slides were immersed in a bifunctional linker solution of 25% glutaraldehyde (GA; C₅H₈O₂; Sigma-Aldrich), incubated at room temperature for 6 h, and then washed in ultrapure water. Finally, four 1 μl droplets of Cy5-conjugated streptavidin (GE Healthcare, absorption peak at 646 nm, emission peak at 664 nm) at a concentration of 10 μg ml⁻¹ were hand-spotted onto the PCs, NR-coated glass slides and reference glass slides by using a pipette. The spots of liquid were allowed to incubate on the surface at 4 °C for 24 h, followed by a final washing step and drying in N₂.

2.3. Device simulation

A commercial software package employing rigorous coupled-wave analysis (RCWA, R-Soft DiffractMOD) was used to study the characteristic response of PCs based on physical parameters of a PC structure such as grating period (Λ), grating depth (d), SiO₂ thickness (t_{SiO_2}), TiO₂ NR-structured thickness (t_{nanorod}), and material RI (n_{UVCP} , n_{SiO_2} and n_{TiO_2}) derived from section 2.1. To accurately obtain the value of the resonant wavelengths, we take into account the fact that both surface chemistry and hand-spotted Cy5-conjugated streptavidin on the PC surface also increase the effective RI of the resonant mode of the PC, resulting in a resonant wavelength shift in the measured transmission spectra. Accordingly, TiO₂ thickness (t_{TiO_2}) was set as 147 nm to compensate for this effect based on the experimental data that adding an additional 1 nm thickness of a dense TiO₂ layer results in a TM resonant wavelength shift of ~1 nm and that a TM resonant wavelength shift of ~7 nm arises from both surface chemistry and hand-spotting Cy5-conjugated streptavidin. Periodic boundary conditions were applied in the x direction, while the y direction was invariant. The TiO₂ NR-structured film was modeled as a uniform layer with a constant n_{nanorod} for all t_{nanorod} since its feature size is much smaller than the resonant wavelengths, indicating that Mie and Rayleigh scattering can be ignored [4]. Only electric-field components are considered in this study since fluorescence processes mainly involve electric dipole oscillations.

2.4. Spectral measurements

A transmission set-up was used to monitor the peak wavelength value (PWV) of resonant reflection of the PC after adding each material onto the PC surface. The measured transmission spectrum has a transmittance minimum (dip) corresponding to a resonant reflectance maximum (peak) at the resonant wavelength. The PC was mounted on an angular adjustment

stage to allow rotation perpendicular to the incident light beam. A broadband tungsten-halogen lamp (Ocean Optics) connected to an optical fiber with a collimator lens was then used as the incident light source to illuminate the PC through a linear polarizer so that either the TM or TE resonance can be excited. The transmitted light was collected using a second optical fiber through a collimator lens, and fed into a spectrometer (USB 2000, Ocean Optics). In order to examine the angular dependence of PC resonant coupling, an experimental set-up similar to the transmission set-up but using an HeNe ($\lambda = 632.8$ nm) laser, a rotational stage and a power meter was used to measure power transmittance as a function of the incident angle (θ) under TM-polarized HeNe laser illumination (figure 2(d), inset).

2.5. Fluorescence intensity measurements

Fluorescence intensity measurements were gathered using a commercially available confocal microarray scanner (LS Reloaded, Tecan) equipped with a TM-polarized HeNe laser ($\lambda = 632.8$ nm), an emission filter centered at $\lambda = 690$ nm with a bandwidth of $\Delta\lambda = 40$ nm (Semrock) and a user-adjustable angle of incident laser excitation to allow matching of the PC TM resonance with the incident laser wavelength. All PC slides, NR-coated glass slides and reference glass slides were scanned with identical parameters (pinhole, photomultiplier tube gain and resolution).

3. Results and discussion

Figure 2(a) shows the simulated PC transmission spectra as a function of wavelength at normal incidence under TM-polarized light illumination (i.e. polarized on the x - z plane, as shown in figure 1(a)) and TE-polarized light illumination (i.e. polarized along the y axis). The simulated TM resonant wavelength was $\lambda_{\text{TM}} = 633$ nm with $\text{FWHM}_{\text{TM}} = 1.2$ nm while the simulated TE resonant wavelength was $\lambda_{\text{TE}} = 682$ nm with $\text{FWHM}_{\text{TE}} = 38$ nm. At normal incidence, the relationship between the resonant wavelength (λ) and the grating period (Λ) can be expressed by the second-order Bragg condition

$$\lambda = n_{\text{eff}}\Lambda \quad (1)$$

where n_{eff} is the effective RI of the resonant mode in the effective TiO₂ layer. Therefore, the effective RI of the TM resonance was $n_{\text{TM}} = 1.758$ for $\lambda_{\text{TM}} = 633$ nm and the effective RI of the TE resonance was $n_{\text{TE}} = 1.894$ for $\lambda_{\text{TE}} = 682$ nm. The effective RI of the TM resonant mode is lower than that of the TE resonant mode because the energy of the TM resonant mode is distributed within the lower RI NR structure to a greater extent, as shown in figure 3. The resulting simulated Q factor of resonant modes are $Q_{\text{TM}} = 527$ and $Q_{\text{TE}} = 18$ based on simulated resonant wavelengths and linewidths.

Figure 2(b) (curves (i)–(iv)) shows the measured PC transmission spectra after addition of successive material coating steps at normal incidence under TM-polarized white light illumination. Figure 2(b)(i) shows that the initial structure without NR deposition has a resonant wavelength of 592.41 nm with an FWHM of 8.16 nm. After the TiO₂ NR deposition,

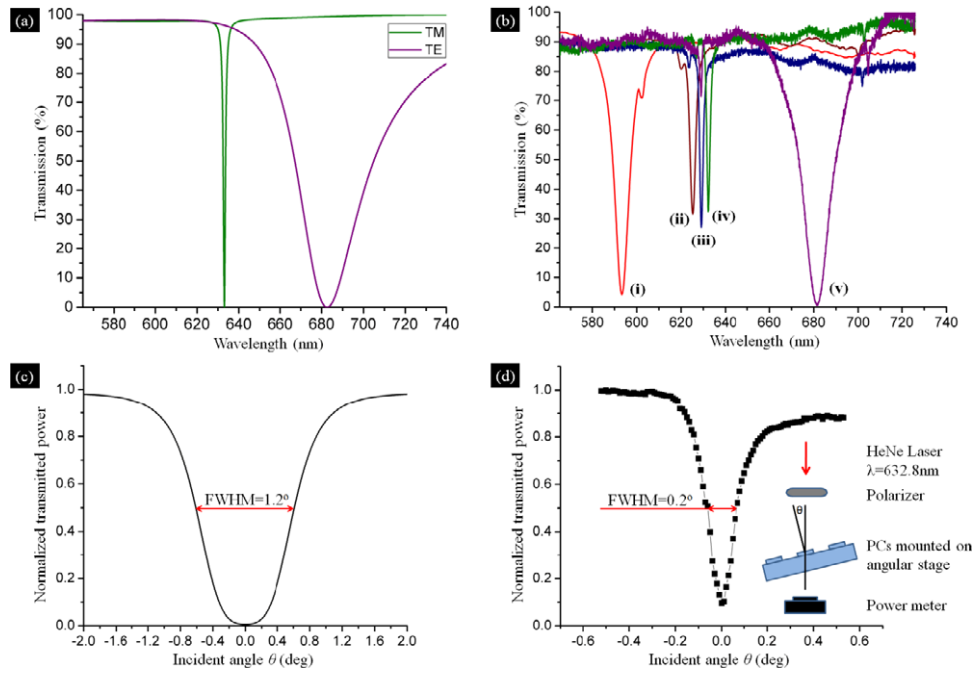


Figure 2. (a) The simulated PC transmission spectra as a function of wavelength at normal incidence under TM-polarized and TE-polarized light illumination. (b) The measured PC transmission spectra after addition of successive material coating steps at normal incidence under TM-polarized white light illumination. (i) The initial structure without NR deposition and spectral shifts of the resonance dip due to (ii) NR deposition, (iii) surface chemistry processes and (iv) hand-spotting Cy5, respectively. (iv) and (v) indicate the final transmission curves under TM-polarized and TE-polarized white light illumination and correspond to TM and TE curves in (a), respectively. (c) The simulated and (d) measured PC normalized transmitted power as a function of incident angle for a TM-polarized incident plane wave and under TM-polarized HeNe laser illumination, respectively. The inset shows the measurement set-up.

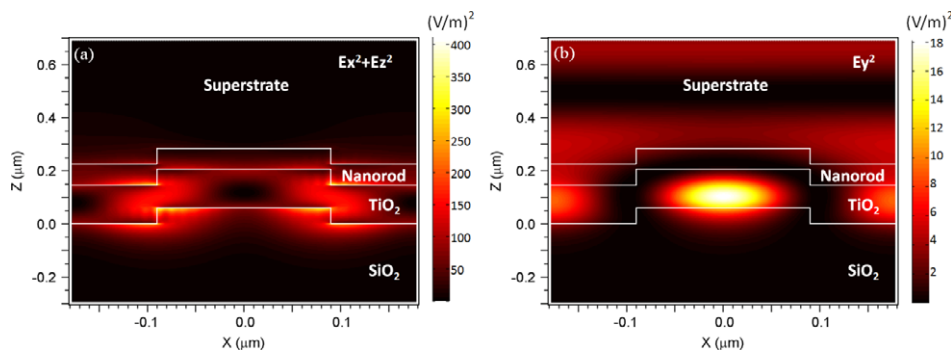


Figure 3. The simulated PC near-electric-field intensity profiles (E^2) for a normally unit incident plane wave for (a) the resonant mode at $\lambda_{TM} = 633$ nm for TM-polarized incidence and (b) the resonant mode at $\lambda_{TE} = 682$ nm for TE-polarized incidence. The color scale associated with each figure represents the intensity of the electric field and is normalized to the unit intensity incident wave.

the change in the superstrate from air ($n_{air} = 1$) to a porous NR structure ($n_{nanorod} = 1.46$) leads to the decrease of the RI contrast relative to a dense nonporous high RI TiO_2 layer ($n_{TiO_2} = 2.3$). This in turn results in a narrower FWHM of 3.62 nm as well as a large PWV shift of 32.78 nm, as shown in figure 2(b)(ii). The surface chemistry leads to an additional PWV shift of 3.87 nm and an FWHM of 2.06 nm because it increases the effective RI of the TM resonant mode, as shown in figure 2(b)(iii). After hand-spotting Cy5-conjugated streptavidin on the PC surface, the final TM resonant wavelength was $\lambda_{TM} = 632.18$ nm with $FWHM_{TM} = 2.05$ nm ($Q_{TM} = 308$) for TM-polarized light illumination and the final TE resonant wavelength was $\lambda_{TE} = 681.36$ nm with $FWHM_{TE} = 17.3$ nm ($Q_{TE} = 39$) for TE-polarized

light illumination, as shown in figure 2(b) curves (iv) and (v), corresponding to TM and TE curves in (a), respectively. The TM resonant wavelength of 632.18 nm closely matched the HeNe laser wavelength ($\lambda = 632.8$ nm) as well as the simulated TM resonant wavelength of 633 nm. More importantly, TM and TE resonances overlap the absorption and emission spectra of Cy-5, respectively. Compared with our previous work which utilized only the TE resonance for excitation [4, 14], this PC possesses a higher Q factor, $Q \sim 308$, in TM resonance.

Figures 2(c) and (d) show simulated and measured PC normalized transmitted power as a function of the angle of incidence (θ) for a TM-polarized incident plane wave ($\lambda_{TM} = 633$ nm) and under TM-polarized HeNe laser ($\lambda = 632.8$ nm)

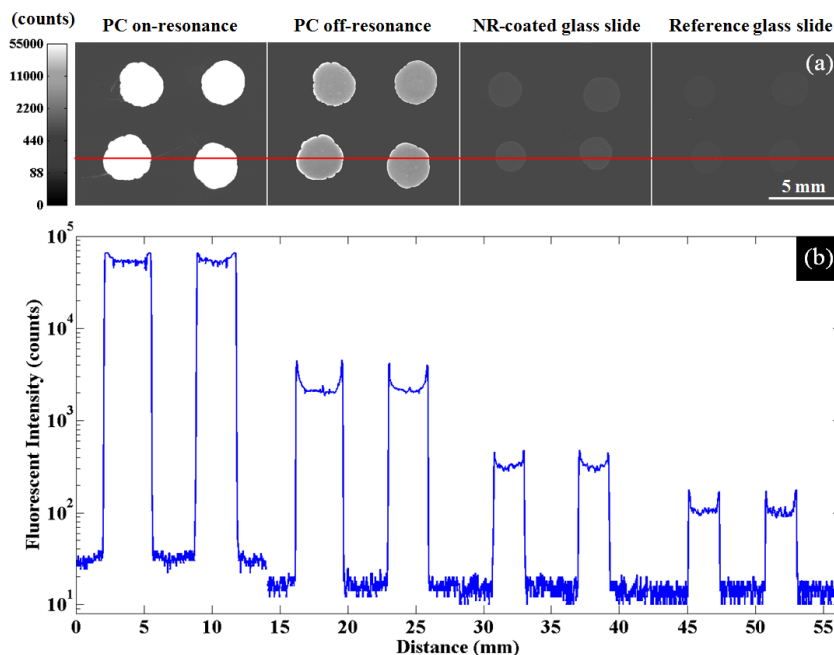


Figure 4. (a) Fluorescence images of Cy5-conjugated streptavidin spots for the PC with on- ($\theta = 0^\circ$) and off- ($\theta = 20^\circ$) resonance conditions, the NR-coated glass slide ($\theta = 0^\circ$) and the reference glass slide ($\theta = 0^\circ$). The color scale represents the fluorescent intensity. (b) Corresponding line profiles for a cross section of fluorescent spots (red line in (a)) plotted on a logarithmic scale.

illumination, respectively. Both simulation and experiment show that the coupling efficiency of the PC is sensitive to the angle orientation of the incident light. Maximum coupling efficiency occurs at the dip in transmitted power where the incident angle corresponds to the resonant angle, in this case, at $\theta = 0^\circ$. TM resonance is observable over a short range of angles centered at normal incidence, as the FWHM of 1.2° for simulation and FWHM of 0.2° for experiment, respectively. The discrepancy between measured and simulated Q factor likely arises because the simulation model does not take into account the rounding and sidewall deposition that occurs during dielectric film sputtering which affects the duty cycle. Our model also does not account for the wavelength dependence of RI.

Since the fluorophore excitation rate is proportional to the near-electric-field intensity [17, 18], the fluorescence enhancement can be estimated by calculating the square of the amplitude of the near-electric field at the surface of the PC. Figures 3(a) and (b) show the simulated PC near-electric-field intensity profiles (E^2) for a normally unit incident plane wave for the resonant mode at $\lambda_{\text{TM}} = 633$ nm for TM-polarized incidence and the resonant mode at $\lambda_{\text{TE}} = 682$ nm for TE-polarized incidence, respectively. For the TM resonance case, the continuity requirements of the displacement field at the interface between the lower RI NR structure and the higher RI TiO_2 layer indicates that the greater electric field appears in the low RI NR structure rather than in the high RI TiO_2 layer, and therefore most intense near-electric-field intensities concentrate within the NR structure, in contrast to the TE resonance case. Since the TM resonance spatially extends into both the low RI NR structure and the high RI TiO_2 layer, it has a lower effective RI than the TE resonance. The spatial average of E^2 within the whole NR volume and 20 nm above the NR

surface was calculated to be 66.6 and 39.0 (V m^{-1})² for the TM resonant mode as compared to 2.0 and 3.1 (V m^{-1})² for the TE resonant mode. Consequently, it is obvious from these calculations that the fluorophore excitation rate can be greatly increased if the PC is engineered for a high- Q TM resonant condition to provide enhanced excitation. In addition, the TM resonance extends more fully into the superstrate media than the TE resonance, resulting in more effective resonant coupling to adsorbed fluorophores.

Figure 4(a) shows scanned fluorescent images of the PC under on/off-resonance conditions, the NR-coated glass slide and the reference glass slide with a dense 20 nm TiO_2 coating. For PC slides, the on-resonance condition occurs when $\theta = 0^\circ$ because the TM resonant wavelength of 632.18 nm closely coincides with the laser wavelength of 632.8 nm, while 20° is defined as off-resonance where the TM resonant wavelength is far away from the laser wavelength. For the glass reference slides, there is no scan angle dependence since no resonant condition exists, and hence we choose $\theta = 0^\circ$ as the scan angle. Once digital image files were obtained, Array-Pro Analyzer software was used to quantify spot and background fluorescence intensities and Matlab software was used to read the image files to generate corresponding line profiles of the fluorescence intensity across all spots, as plotted on a logarithmic scale in figure 4(b).

Table 1 lists the quantitative results of the fluorescence measurements of figure 4 for PC on-resonance ($\theta = 0^\circ$) and off-resonance ($\theta = 20^\circ$), the NR-coated glass slide ($\theta = 0^\circ$) and the reference glass slide ($\theta = 0^\circ$). For each spot shown in figure 4, the net fluorescence intensity was calculated by the spot intensity minus the local background intensity. After subtracting the background, the mean spot intensity for the

Table 1. Raw spot and background intensities for the PC with on- ($\theta = 0^\circ$) and off- ($\theta = 20^\circ$) resonance conditions, the NR-coated glass slide ($\theta = 0^\circ$) and the reference glass slide ($\theta = 0^\circ$). After subtracting the background intensity, the enhancement factors are determined.

PC ($\theta = 0^\circ$) (S1)	Spot intensities (counts)				Background intensities (counts)				Enhancement factors			
	PC ($\theta = 20^\circ$) (S2)	NR glass ($\theta = 0^\circ$) (S3)	Glass ($\theta = 0^\circ$) (S4)		PC ($\theta = 0^\circ$) (B1)	PC ($\theta = 20^\circ$) (B2)	NR glass ($\theta = 0^\circ$) (B3)	Glass ($\theta = 0^\circ$) (B4)	PC-on/ PC-off = (S1-B1)/ (S2-B2)	PC-off/ NR glass = (S2-B2)/ (S3-B3)	NR glass/ glass = (S3-B3)/ (S4-B4)	PC-on/ glass = (S1-B1)/ (S4-B4)
	$51\,019 \pm 2792$	2055 ± 72	334 ± 20	99 ± 7	30 ± 3	16 ± 2	14 ± 2	12 ± 2	25 ± 1.3	6.4 ± 0.4	3.7 ± 0.3	588 ± 45.8

PC at the on-resonance condition was enhanced by $588\times$ relative to that for the reference glass slide. We attribute this enhancement mainly to the product of the enhanced excitation effect, the enhanced extraction effect and the enhanced surface area provided by the NR coating, which can be expressed by the following equation:

$$\frac{\text{PC(on res)}}{\text{glass}} = \frac{\text{PC(on res)}}{\text{PC(off res)}} \times \frac{\text{PC(off res)}}{\text{NR glass}} \times \frac{\text{NR glass}}{\text{glass}}. \quad (2)$$

The magnitude of the enhanced excitation effect can be measured by the ratio of fluorescent intensity for PC on-resonance versus PC off-resonance because the enhanced near-electric field is only active when the PC is illuminated in the on-resonance condition. Enhanced excitation can be attributed to the enhanced near-electric-field intensity (E^2) of the TM resonant mode used to excite the fluorophores and the spatial distribution of the TM mode within the NR volume, where adsorption of fluorescent species occurs. For the TM resonance, the most intense E^2 is distributed in the proximity of the porous NR surface rather than within the dense nonporous high RI TiO_2 layer [4, 14]. Furthermore, average E^2 is proportional to the Q factor at the resonant wavelength, and therefore these TM resonant characteristics will efficiently excite Cy5 in the vicinity of the porous NR material. The magnitude of the enhanced extraction effect can be measured by the ratio of fluorescent intensity for PC off-resonance versus the NR-coated glass surface because no near-electric field is created to stimulate Cy5 when the PC is operated in the off-resonance condition. Enhanced extraction results from the redirection of TE-polarized fluorescence emitted by Cy5 towards the detection instrument via coupling to the TE resonant mode of the PC, which is designed to spectrally overlap the emission spectrum of Cy5. Therefore, through the use of a low- Q TE resonance, the bandwidth of the TE resonance of the PC roughly matches the emission spectrum of Cy5. The contribution of the enhanced surface area effect to the overall enhancement factor can be determined by the ratio of fluorescent intensity for NR-coated glass surface versus the unpatterned reference surface, which indicates that the porous NR structure provides $3.7\times$ more surface area available for fluorophore-PC interaction. This surface area enhancement is similar to that previously characterized (reported) for similar NR films [15].

4. Conclusion

We have experimentally demonstrated that a linear grating PC surface incorporating a highly porous NR-structured TiO_2

layer exhibits fluorescence enhancement of up to $588\times$ in comparison to an unpatterned glass slide. The enhancement is derived through the use of a high- Q TM resonance for excitation of Cy5 and a low- Q TE resonance for the extraction of emission from Cy5, in combination with a large, highly porous surface area that allows fluorophores to penetrate and increase the interaction of adsorbed fluorophores with the volume adjacent to the PC surface where fluorophore-PC interaction is strongest. This significant increase in fluorescence enhancement enables better fluorescence detection sensitivity for a wide range of fluorescence-based assays such as gene expression assays and protein biomarker assays than an assay on an optically passive substrate.

Acknowledgments

This work was supported by the National Institutes of Health (GM086382A), the National Science Foundation (CBET 07-54122) and SRU Biosystems. Any opinions, findings, conclusions or recommendations expressed in this material are those of the authors and do not necessarily reflect the views of the National Institutes of Health or the National Science Foundation. The authors thank the staff at the Micro and Nanotechnology Laboratory at the University of Illinois at Urbana-Champaign. H-Y Wu and W Zhang contributed equally to this paper.

References

- [1] Hung Y J, Smolyaninov I I and Davis C C 2006 *Opt. Express* **14** 10825–30
- [2] Aslan K, Malyn S N and Geddes C D 2007 *J. Fluoresc.* **17** 7–13
- [3] Lakowicz J R 2001 *Anal. Biochem.* **298** 1–24
- [4] Zhang W, Ganesh N, Mathias P C and Cunningham B T 2008 *Small* **4** 2199–203
- [5] Lakowicz J R 2006 *Plasmonics* **1** 5–33
- [6] Abdulhalim I, Karabchevsky A, Patzig C, Rauschenbach B, Fuhrmann B, Eltzov E, Marks R, Xu J, Zhang F and Lakhtakia A 2009 *Appl. Phys. Lett.* **94** 063106
- [7] Bardhan R, Grady N K, Cole J R, Joshi A and Halas N J 2009 *ACS Nano* **3** 744–52
- [8] Mathias P C, Wu H Y and Cunningham B T 2009 *Appl. Phys. Lett.* **95** 021111
- [9] Dobbs D W, Gershkovich I and Cunningham B T 2006 *Appl. Phys. Lett.* **89** 123113
- [10] Budach W, Neuschafer D, Wanke C and Chibout S D 2003 *Anal. Chem.* **75** 2571–7
- [11] Mathias P C, Ganesh N and Cunningham B T 2009 *Anal. Chem.* **80** 9013–20

- [12] Ganesh N, Zhang W, Mathias P C, Chow E, Soares J A N T, Malyarchuk V, Smith A D and Cunningham B T 2007 *Nat. Nanotechnol.* **2** 515–20
- [13] Rosenblatt D, Sharon A and Friesem A A 1997 *IEEE J. Quantum Electron.* **33** 2038–59
- [14] Zhang W and Cunningham B T 2008 *Appl. Phys. Lett.* **93** 133115
- [15] Zhang W, Ganesh N, Block I D and Cunningham B T 2008 *Sensors Actuators B* **131** 279–84
- [16] Kim S-M, Zhang W and Cunningham B T 2008 *Appl. Phys. Lett.* **93** 143112
- [17] Weitz D A, Garoff S, Gersten J I and Nitzan A 1983 *J. Chem. Phys.* **78** 5324–88
- [18] Anger P, Bharadwaj P and Novotny L 2006 *Phys. Rev. Lett.* **96** 113002